arXiv:1411.3807v1 [cond-mat.stat-mech] 14 Nov 2014

A cluster algorithm for Monte Carlo simulations of spin ice

Hiromi Otsuka
Department of Physics, Tokyo Metropolitan University, Tokyo 192-0397, Japan
(Dated: November 17, 2014)

We present an algorithm for Monte Carlo simulations of a nearest-neighbor spin ice model based on its cluster representation. To assess its performance, we estimate a relaxation time, and find that, in contrast to the Metropolis algorithm, our algorithm does not develop spin-freezing. Also, to demonstrate the efficiency, we calculate the spin and charge structure factors, and observe pinch points in a high-resolution color map. We then find that Debye screening works among defects and brings about short-range correlations, and that the deconfinement transition triggered by a fugacity of defects z is dictated by a singular part of the free-energy density $f_{\rm s} \propto z$.

PACS numbers: 75.10.Hk, 75.50.Mm, 05.10.Ln

The pyrochlore lattice $\Lambda_{\rm p}$ (Fig. 1) is one of the more important structures in condensed matters physics [1] because inherent frustrations can inhibit the stabilization of conventional phases, and also not a few numbers of pyrochlores have been synthesized and have provided measurements of their static and dynamical properties. The so-called spin ice materials $Ho_2Ti_2O_7$ [2] and $Dy_2Ti_2O_7$ [3] are examples; despite their large magnetic moments, they were found not to be magnetically ordered, but to exhibit a residual entropy. Moreover, with the intriguing proposal of magnetic monopolelike excitations in these materials [4], intensive efforts have been paid to account for their unconventional phases and exotic excitations near the ground states [5–15].

In general, numerical approaches can play an important role in this developing research area; indeed, efficient methods have also been sought for spin ice. The Monte Carlo (MC) method is apparently of principal importance, but the single-spin flip dynamics based on the Metropolis algorithm is inefficient at lower temperatures due to spin-freezing [7]. This indicates that we should employ spin-flip dynamics compatible with the ice rule [16], which we shall soon discuss. In studies of vertex models for water ice, Barkema and Newman closely discussed multi-spin-flip algorithms using loop clusters of spins [17]. Based on their discussion, Melko *et al.* introduced loop flips into the Metropolis algorithm, and succeeded in simulating a spin-ice model at lower temperatures [7]. Jaubert *et al.* re-expressed the local Boltzmann weight as a sum of graph weights, and constructed a loop cluster which can be freely flipped (worm algorithm) [9]. Also, more resent research reported loop-update MC studies on other types of pyrochlore magnets [18].

In this rapid communication we propose a MC algorithm for a simple spin-ice model based on its cluster representation. Significantly, the algorithm is quite efficient in simulations for all temperatures, and thus provides us an opportunity to simulate large systems very accurately; indeed this is necessary for studies on phase transitions and critical phenomena as we see below. Also, our algorithm is simple in that it could provide a building block for simulations of more complicated systems including dipolar spin ices. In what follows, we shall detail our algorithm and provide numerical results.

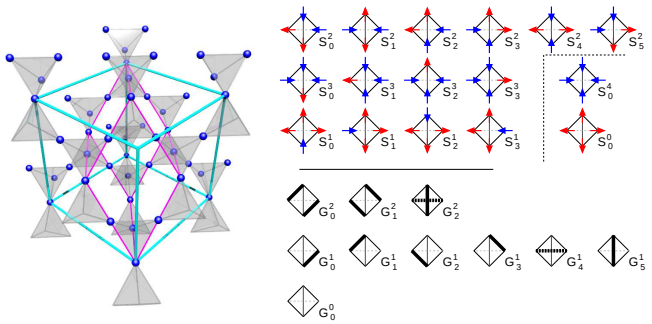

FIG. 1. (Color online) Left: The pyrochlore lattice $\Lambda_{\rm p}$. Blue dots represent magnetic ions. The frame in magenta (cyan) marks the primitive (cubic) cell with 4 (16) spins. The edge length and fundamental vectors of the cubic cell are, respectively, a and $(\mathbf{e}_x, \mathbf{e}_y, \mathbf{e}_z)$. The length of primitive vectors, e.g., $\mathbf{t}_1 = \frac{a}{2}(\mathbf{e}_x + \mathbf{e}_y)$ is $a/\sqrt{2}$. Right: Top three lines give the 16 states per one tetrahedron S_u^μ classified by the number of inward spins μ (blue arrows). Bottom three lines give the 10 graphs G_v^ν, where ν denotes the number of bonds (bold lines).

Model: Suppose that p specifies a site in $\Lambda_{\rm p}$ and that the unit vectors for the local axes $\hat{\mathbf{u}}(p)$ and the Ising variables $\sigma(p) = \pm 1$ define the magnetic moments as $\mathbf{S}(p) = \hat{\mathbf{u}}(p)\sigma(p)$. Then, the simplest model is given by a Hamiltonian with nearest-neighbor (NN) coupling J:

$$H_{\rm SI} = -3J \sum_{\langle p,p' \rangle} \mathbf{S}(p) \cdot \mathbf{S}(p') = J \sum_{\langle p,p' \rangle} \sigma(p)\sigma(p'). \quad (1)$$

We used the relation $\hat{\mathbf{u}}(p) \cdot \hat{\mathbf{u}}(p') = -\frac{1}{3}$ for NN spins. Because of this anisotropy, an effective ferromagnetic model [5] is reduced to a fully-frustrated Ising model [19, 20] for which the ground state consists of tetrahedra satisfying the "two in-two out" condition (the ice rule [16]), and exhibits Pauling's entropy. For later convenience, we also define the diamond lattice $\Lambda_{\rm d}$ whose site (d) sits at the center of each tetrahedron, and introduce a quantity $\rho(d) := \eta(d) \sum_{\{p_d\}} \sigma(p_d)/2$. $\{p_d\}$ denotes a set of

nearest-neighboring sites to d, and the factor $\eta(d) = \pm 1$ is assigned to the sublattices of $\Lambda_{\rm d}$ to which d belongs. $\rho(d)$ is nonzero for tetrahedra not satisfying the ice rule, and can be regarded as the charge of point defects (i.e., the magnetic monopolelike excitations).

Algorithm: We start with a definition of the local Boltzmann weights, and then introduce graphs. Let S_u^μ stand for the 16 states per tetrahedron, where $\mu \in [0, 4]$ is the number of inward spins, thereby specifying the class, and u is the member index in that class (see Fig. 1). Then, the local Boltzmann weight $\omega(S_u^\mu)$ is independent of u, and further $\omega(S_u^4) = \omega(S_u^0) = z^4$, $\omega(S_u^3) = \omega(S_u^1) = z$, and $\omega(S_u^2) = 1$, where $z := \exp(-2/T)$ (we choose the lowest energy per tetrahedron, $-2J$, as an origin, and measure the temperature T in units of $J/k_{\rm B}$). Following the Fortuin-Kasteleyn argument [21], we re-express the system as a superposition of random clusters with positive coefficients. Because the spin configurations are two in-two out in the ice manifold, the transition graphs between any two of them are loop-gas-like. We thus expect emerging clusters to form loops at lower T [22]. This condition is satisfied if only inward-outward pairs of spins *can* be linked by bonds, just like two Ising spins being energetically satisfied in the Swendsen-Wang (SW) algorithm [23]. To give this concept shape, we introduce the 10 graphs G_v^ν (see Fig. 1) classified by a number of bonds $\nu \in [0, 2]$ (v indexes members in the class), and consider the following weight decomposition equation [24, 25]:

$$\omega(S_u^\mu) = \sum_{\nu,v} \Delta(S_u^\mu, G_v^\nu) W(G_v^\nu), \tag{2}$$

where $W(G_v^\nu) \geq 0$ are graph weights to be determined. Here, we have introduced the factor $\Delta(S_u^\mu, G_v^\nu) = 0$ or 1 to express *compatibility* between states and graphs under the abovementioned condition: For instance, for a given state S_0^1, $\Delta(S_0^1, G_0^1) = \Delta(S_0^1, G_2^1) = \Delta(S_0^1, G_5^1) = \Delta(S_0^1, G_0^0) = 1$, and 0 otherwise. This factor ensures that the system is decomposed into a mixture of independent loops and strings composed of spins directed along their lines. Once the graph weights satisfying Eq. (2) are given, we can then express the conditional probability to assign a graph to the tetrahedron in a given state as $\Pr(G_v^\nu | S_u^\mu) = \Delta(S_u^\mu, G_v^\nu) W(G_v^\nu)/w(S_u^\mu)$. Because Eq. (2) is underdetermined, it is necessary to search for a solution guided by the symmetries: As the Boltzmann weights are independent of u, i.e., $\omega(S_u^\mu) =: \omega^\mu$, we also assume that the graph weights are independent of v, i.e., $W^\nu := W(G_v^\nu)$. Then, Eq. (2) is reduced to $\omega^\mu = \sum_\nu \Gamma^{\mu\nu} W^\nu$, where $\Gamma^{\mu\nu} := \sum_v \Delta(S_u^\mu, G_v^\nu)$ is independent of u. The reduced equations are now straightforward to solve; we obtain the following solution:

$$W^0 = z^4, \quad W^1 = \frac{z - z^4}{3}, \quad W^2 = \frac{3 - 4z + z^4}{6}. \tag{3}$$

For the reader's convenience, we have summarized the details of our formulation in Supplemental Material.

Here, some comments are in order: First, in general, the equations such as Eq. (2) do not always possess positive solutions for all parameter region, and sometimes we should divide the region into parts, in each of which a proper choice of graphs is necessary to obtain positive solution. Meanwhile, Eq. (3) is positive definite, and can be used in simulations for all T to generate spin configurations according to the Boltzmann weight. Second, the ergodicity condition obviously holds at finite T because the zero-bond graph weight W^0 is nonzero for all S_u^μ (see Supplemental Material), and thus an arbitrary spin configuration can be realized with nonvanishing probability. At $T = 0$, any two configurations, as abovementioned, are connected by the transition graphs consisting of loops [22]. In our cluster decomposition, only two-bond graphs G_v^2 engage ($W^\nu = \frac{1}{2}\delta_{\nu 2}$), so our algorithm reduces to the standard loop algorithm for ice models [17, 26]. Therefore, the updates via loops so created can realize any spin configurations also in the ice manifold. Third, a short explanation of the improved estimators [27] is given by taking an Ising spin correlation $\mathcal{S}(p, p') := \langle \sigma(p)\sigma(p') \rangle$ as an example. Like the SW algorithm, we decompose the whole system into a set of clusters $\{\mathcal{L}_1, \cdots, \mathcal{L}_m\}$. So, we can improve the estimators by taking an average over the 2^m spin configurations by hand which are virtually created by applying transition graphs made of $\{\mathcal{L}\}$ to a spin configuration in the Markov chain. Because of the randomness of clusters and the nature of the observable $\sigma(p)\sigma(p')$, the resulting expression is simply given as

$$[\sigma(p)\sigma(p')]_{\rm impr} = \delta(p, p' | \{\mathcal{L}\}) \sigma(p)\sigma(p'), \tag{4}$$

where $\delta(p, p' | \{\mathcal{L}\}) = 1$ if two sites are on the same cluster, and 0 otherwise. Further, $\sigma(p)\sigma(p')$ only depends on the even-odd parity of the distance between two spins along the line. Because the spin correlation function is the most fundamental quantity, we benefit from Eq. (4) in calculations of other physical quantities. Indeed, we discuss the defect charge correlation $\mathcal{C}(d, d') := -\langle \rho(d)\rho(d') \rangle$, whose observable is also improved as $[\rho(d)\rho(d')]_{\rm impr} = \eta(d)\eta(d') \sum_{\{p_d\}\{p_{d'}\}} [\sigma(p_d)\sigma(p_{d'})]_{\rm impr}/4$. This expression is much more efficient than the enumeration of $\mathcal{C}$ via $\rho(d)$.

Performance: We shall now assess the performance of our algorithm. More explicitly, we estimate equilibrium relaxation times observed in the Metropolis and the cluster algorithms, and compare them for various T. In doing this, it is important to choose a proper quantity to characterize the relaxation. Our model Eq. (1) is known not to order at any T, but exhibits cooperative paramagnetic behavior of diverging susceptibility [8, 13]. Therefore, we measure the relaxation times τ via fluctuations of the uniform magnetization $M := \sum_p \mathbf{e}_z \cdot \mathbf{S}(p)$ [12]. First, we calculate the time-displaced auto-correlation function of M: Define one MC step (MCS) as $|\Lambda_{\rm p}|$ successive MC trials giving a unit of time for the MC dynamics [28], and denote a measurement of M at a lth MCS as $M(l)$. The correlation function is then given

as $A_M(k) = \langle M(k+l)M(l)\rangle$. In Fig. 2(a), we provide $\bar{A}_M(k) = A_M(k)/A_M(0)$ obtained by the two algorithms. The system with a linear dimension $L = 64$ ($|\Lambda_{\rm p}| = 4L^3$) is simulated at $T = 0.3$ (circles), 0.5 (diamonds), and 1.0 (triangles). Then, we observe a simple relaxation in the Metropolis dynamics, so we can evaluate τ via fitting the data points (see blue marks with solid curves). In contrast, the relaxation in the cluster dynamics given by red marks is very quick so that we cannot evaluate τ from these plots. To put forward our performance analysis, we next employ the statistical-dependence-time (SDT) approach [29, 30] which only requires statistical quantities, instead of the time-displaced correlation and data fitting. The SDT is defined as a ratio of two-types of variances σ^2 and $(\delta M)^2_n$: The former is an uniform magnetic susceptibility (multiplied by T), and is algorithm independent. However, the latter is a variance of statistically independent short-time averages with a given bin length n: $\langle M_\alpha\rangle_n = \frac{1}{n}\sum_{k=1}^{n} M_\alpha(k)$ and $(\delta M)^2_n = \frac{1}{N}\sum_{\alpha=1}^{N}\langle M_\alpha\rangle^2_n$. N is a number of independent runs, and is supposed to be large (e.g., $N = 2304$ in our calculation). Then, the ratio, $\tau_{\rm dep} := n(\delta M)^2_n/2\sigma^2$, defines SDT, and estimates τ in the limit $n \nearrow \infty$ [29]. We plot the n dependence of $\tau_{\rm dep}$ in Fig. 2(b). We find a convergence of the data as bin length increases, and further, for the Metropolis algorithm, the limiting values agree well with the relaxation times estimated from $A_M(k)$ (blue dotted lines) demonstrating a reliability of the SDT approach [29]. Meanwhile, the cluster algorithm exhibits $\tau_{\rm dep} \simeq \frac{1}{2}$ (red dotted line) that is independent of n and T. This implies, assuming single mode relaxation, a vanishing of τ for all T [29]. In Fig. 2(c), we also check the system-size dependence of $\tau_{\rm dep}$ up to $L = 64$ at maximum bin lengths $n_{\rm max}(T)$, and confirm its absence in these data. Finally, in Fig. 2(d), we compare T dependence of τ estimated via $\tau_{\rm dep}$. Although the relaxation time increases as $\tau_{\rm M} \propto \exp(2.1/T)$ for the Metropolis algorithm, it is the constant $\frac{1}{2}$ indicating $\tau_{\rm C} = 0$ in the cluster algorithm. An energy scale in $\tau_{\rm M}$, $\Delta E \simeq 2.1$, is close to the defect creation energy, so that the relaxation depends on point defects. In contrast, spins bundled in loops and strings can be flipped randomly, and thus the cluster algorithm can update them to completely new configurations. Consequently, spin-freezing inherent in the single-spin-flip Metropolis algorithm is absent in our cluster MC simulations.

Results: We shall now summarize our numerical calculation data; in particular, as a hallmark of the ice system, we first demonstrate the emergence of pinch points in the spin structure factor $\mathcal{S}_\perp(\mathbf{Q})$ [31–33]. This quantity is defined by an average of the squared norm of the Fourier component of spins perpendicular to the wavevector $\mathbf{Q}$, i.e., $\langle\|\hat{\mathbf{Q}}\times\mathbf{S}(\mathbf{Q})\|^2\rangle$, and gives the diffuse neutron scattering intensity (aside from an atomic form factor). Although the pinch-point structure observed in experiments [6] has been reproduced in MC calculations [10, 13], system sizes and temperatures simulated are limited to relatively small and high values, respectively. Therefore, we calculate $\mathcal{S}_\perp(\mathbf{Q})$ for the $L = 256$ system at temperatures down to $T = 0.3$ (for instance, for $Dy_2Ti_2O_7$, 67,108,864 Dy^{3+} at about 0.33 K [5]), and then create a high-resolution scattering-intensity color map. By comparing it with data for a 4,000-spin system given in the loop-update MC study [13], one finds a considerable improvement, and thus a significant development in our MC simulation of spin ice. Also, we calculate the charge structure factor $\mathcal{C}(\mathbf{Q}) = \langle|\rho(\mathbf{Q})|^2\rangle$, and provide information on spatial correlations among defects.

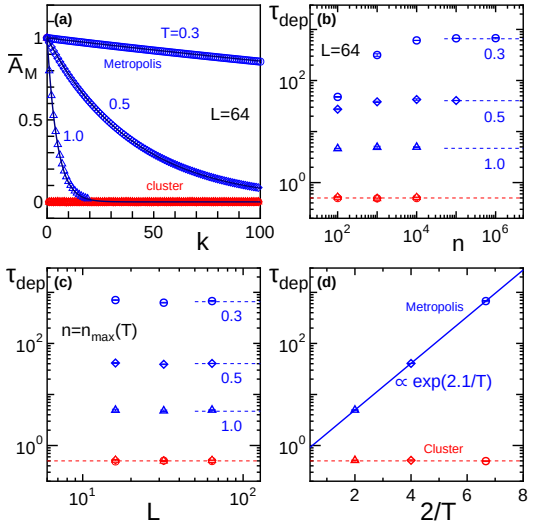

FIG. 2. (Color online) (a): $\bar{A}_M(k)$ at $T = 0.3$, 0.5, and 1.0. Blue (red) marks plot data by the Metropolis (cluster) algorithm. The forms of exponential relaxation are drawn as fitted curves in blue. (b) and (c): The n and L dependencies of $\tau_{\rm dep}$ in two algorithms. The relaxation times estimated via $\bar{A}_M(k)$ are given as blue dotted lines; the red indicate $\tau_{\rm dep} = \frac{1}{2}$. (d): Temperature dependence of the relaxation times; the fitted line shows its exponential dependence in the Metropolis dynamics.

Following a previous study [6], we scan the plane in the dual space to the periodic lattice parametrized by $\mathbf{Q} = (2\pi/a)(h\mathbf{e}_x + h\mathbf{e}_y + l\mathbf{e}_z)$, and conventionally denoted as (h, h, l). Then, reflecting the structure of $\Lambda_{\rm p}$, $\mathcal{S}_\perp(\mathbf{Q})$ taken near some special wavevectors plays a role in measuring the extent to which the ice rule holds. In the left panels of Fig. 3, we display color maps, for which from bottom to top $T = 0.3$, 1.0 and 2.0. At each T, the data are linearly mapped to colors in the bar with its top and bottom colors assigned to the maximum and minimum values. At $T = 0.3$, we can observe the pinch-point structure at (0,0,2), (1,1,1), (2,2,2), and so on, but it becomes increasing unclear as T increases; this reflects the breaking of the ice rule and the increasing of defects. This tendency can be recognized also in the charge structure factor: In the right panels of Fig. 3, we give $\mathcal{C}(\mathbf{Q})$ for the same plane at the same temperatures. We observe sharp spots at lower T and their diffusion with increasing T. In

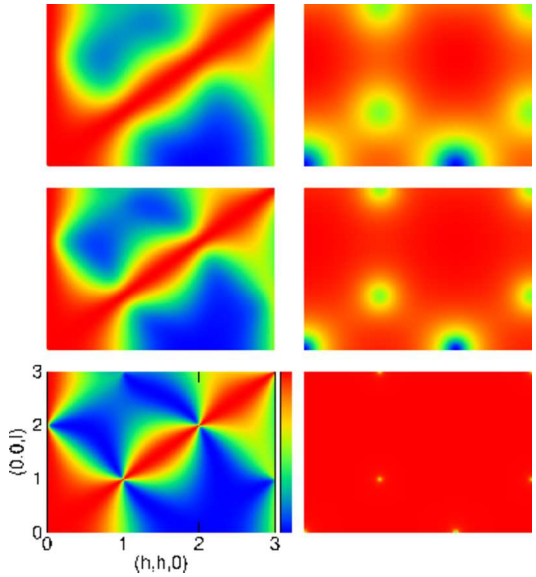

FIG. 3. (Color online) Color maps of spin and charge structure factors, $\mathcal{S}_\perp(\mathbf{Q})$ and $\mathcal{C}(\mathbf{Q})$, at T =0.3 (the bottom), 1.0 (the middle), and 2.0 (the top). The data in the left (right) panels are normalized by an amplitude of spin (charge) structure factor at each T. The wavevector is on the (h, h, l) plane, and is measured in units of $2\pi/a$.

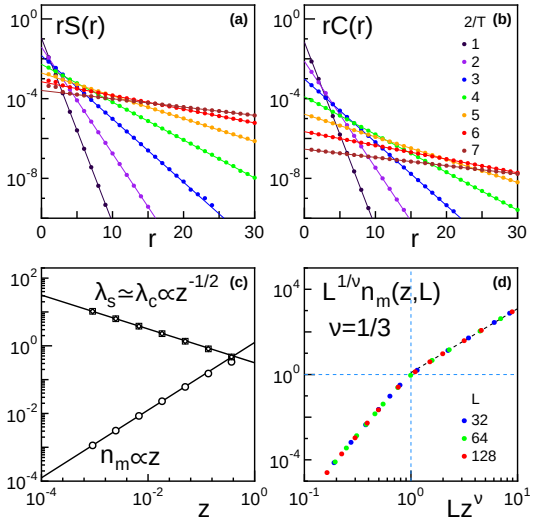

FIG. 4. (Color online) (a) and (b): $r\mathcal{S}$ and $r\mathcal{C}$ versus r for various T. Slopes of fitted lines determine the inverse correlation lengths for the $L = 128$ system. (c): The z dependence of $\lambda_{\rm s}$ (diamonds), $\lambda_{\rm c}$ (squares), and $n_{\rm m}$ (circles). The slope of the line for $\lambda_{\rm s,c}$ is $-\frac{1}{2}$, and for $n_{\rm m}$ is 1. (d) gives the finite-size-scaling plot of $n_{\rm m}$ with the critical exponent $\nu = \frac{1}{3}$.

particular, the one around $(0, 0, 0)$ reflects long-distance properties indicating isotropic short-range charge correlations in real space. Moreover, the radius of the spot, a measure of the inverse charge correlation length $1/\lambda_{\rm c}$, shortens with the decrease of T, and thus of the defect number density $n_{\rm m} := \langle \sum_d |\rho(d)| \rangle / |\Lambda_{\rm d}|$.

To understand the defect distributions, the dumbbell model, i.e., the gas of defects interacting via a Coulomb potential is useful. Castelnovo, Moessner, and Sondhi introduced it into the dipolar spin ice [4], and, based on the Debye-Hückel approximation [34], argued a screening effect for which they obtained a Debye screening length $\propto \sqrt{T/\mu_0 n_{\rm m}}$ (μ_0 is the magnetic permeability) [11]. We also consider a gas of defects interacting via a Coulomb potential, but should take its origin being entropic for Eq. (1) into account, i.e., $V_{\rm ent} \propto T\rho(d)\rho(d')/\|\mathbf{x}(d) - \mathbf{x}(d')\|$ [$\mathbf{x}(d)$ is a position vector of the dth site] [35]. With T replacing μ_0 as coupling constant, their result should read $\lambda_{\rm c} \propto \sqrt{1/n_{\rm m}}$. With the structure factors appearing to follow the prediction, we shall look more closely at the screening effect: Figures 4(a) and 4(b) plot $\mathcal{S}(p, p')$ and $\mathcal{C}(d, d')$ between two sites in the same sublattice; their difference vectors are parallel to a primitive axis, i.e., $\mathbf{x} - \mathbf{x}' = r\mathbf{t}_i$. Because of the high accuracy of the data, $\lambda_{\rm s}$ (a spin correlation length) and $\lambda_{\rm c}$ can be obtained reliably from these plots, from which the results, together with $n_{\rm m}$, are summarized in Fig. 4(c): We then find that $\lambda_{\rm s} \simeq \lambda_{\rm c} \propto z^{-1/2}$ [14] and $n_{\rm m} \propto z$, which confirms the Debye screening in spin ice. Consequently, the Coulomb gas—the emergent picture for spin ice—is efficiently simulated via the cluster updates of spins almost satisfying the ice rule. Finally, to shed light on the deconfinement transition from the Coulomb phase to the cooperative paramagnetic phase at finite T [33], we perform a finite-size-scaling analysis of $n_{\rm m}(z, L)$ in Fig. 4(d). The scaled quantity $L^{1/\nu} n_{\rm m}(z, L)$ versus the scaled variable $L/\xi = Lz^\nu$ for different system sizes is plotted with the exponent $\nu = \frac{1}{3}$, and reveals good scaling characteristics. This exhibits $\xi \propto z^{-1/3} \propto \sqrt[3]{1/n_{\rm m}}$, *the mean distance among defects*, and the singular part of the free-energy density relevant to the deconfinement transition is simply given by $f_{\rm s} \propto \xi^{-3} \propto z$ [33, 36].

Conclusion: We proposed a MC algorithm for spin ice, which decomposes the whole system into a mixture of independent loops and strings. In contrast to the Metropolis algorithm, it is free from spin-freezing; we constructed high-resolution color maps of the structure factors to demonstrate its efficiency. Also, we proffered evidence to support Debye screening in spin ice, and concluded that the mean distance among defects is relevant to the deconfinement transition. Apparently, an extension of our loop-string algorithm applicable to dipolar spin ices is very important. Recently, we have evaluated its possible combined use with the Metropolis algorithm by which the dipolar interactions are treated under the fixed loop-string configurations; we shall report on this topic elsewhere (see also Ref. [18]).

The author thanks H. Takatsu, K. Goto, H. Kadowaki, K. Chie, and Y. Okabe for stimulating discussions. The main computations were performed using the facilities of Cyberscience Center in Tohoku University. This work was supported by JSPS KAKENHI (26400399).

[1] S. T. Bramwell and M. J. P. Gingras, Science **294**, 1495 (2001).

[2] M. J. Harris, S. T. Bramwell, D. F. McMorrow, T. Zeiske, and K. W. Godfrey, Phys. Rev. Lett. **79**, 2554 (1997).

[3] A. P. Ramirez, A. Hayashi, R. J. Cava, R. Siddharthan, and B. S. Shastry, Nature **399**, 333 (1999).

[4] C. Castelnovo, R. Moessner, and S. L. Sondhi, Nature **451**, 42 (2008).

[5] B. C. den Hertog and M. J. P. Gingras, Phys. Rev. Lett. **84**, 3430 (2000).

[6] S. T. Bramwell, M. J. Harris, B. C. den Hertog, M. J. P. Gingras, J. S. Gardner, D. F. McMorrow, A. R. Wildes, A. L. Cornelius, J. D. M. Champion, R. G. Melko, and T. Fennell, Phys. Rev. Lett. **87**, 047205 (2001).

[7] R. G. Melko, B. C. den Hertog, and M. J. P. Gingras, Phys. Rev. Lett. **87**, 067203 (2001).

[8] I. A. Ryzhkin, J. Exp. Theor. Phys. **101**, 481 (2005).

[9] L. D. C. Jaubert, J. T. Chalker, P. C. W. Holdsworth, and R. Moessner, Phys. Rev. Lett. **100**, 067207 (2008).

[10] T. Fennell, P. P. Deen, A. R. Wildes, K. Schmalzl, D. Prabhakaran, A. T. Boothroyd, R. J. Aldus, D. F. McMorrow, and S. T. Bramwell, Science **326**, 415 (2009).

[11] C. Castelnovo, R. Moessner, and S. L. Sondhi, Phys. Rev. B **84**, 144435 (2011).

[12] For relaxation times observed in the self-overlapping correlation, see L. D. C. Jaubert and P. C. W. Holdsworth, J. Phys.: Condens. Matter **23**, 164222 (2011).

[13] L. D. C. Jaubert, M. J. Harris, T. Fennell, R. G. Melko, S. T. Bramwell, and P. C. W. Holdsworth, Phys. Rev. X **3**, 011014 (2013).

[14] A. Sen, R. Moessner, and S. L. Sondhi, Phys. Rev. Lett. **110**, 107202 (2013).

[15] H. Otsuka, H. Takatsu, K. Goto, and H. Kadowaki, Phys. Rev. B **90**, 144428 (2014).

[16] J. D. Bernal and R. H. Fowler, J. Chem. Phys. **1**, 515 (1933).

[17] G. T. Barkema and M. E. J. Newman, Phys. Rev. E **57**, 1155 (1998) and reference therein.

[18] By Ising embedding technique and by combined use with the Metropolis algorithm, loop-update MCs were applied to Heisenberg spin systems with ice-type degeneracy: H. Shinaoka and Y. Motome, Phys. Rev. B **82**, 134420 (2010); H. Shinaoka, Y. Tomita, and Y. Motome, J. Phys.: Conf. Ser. **320**, 012009 (2011).

[19] J. Villain, J. Phys. C **10**, 1717 (1977).

[20] P. W. Anderson, Phys. Rev. **102**, 1008 (1956).

[21] C. M. Fortuin and P. W. Kasteleyn, Physica **57**, 536 (1972).

[22] H. G. Evertz, G. Lana, and M. Marcu, Phys. Rev. Lett. **70**, 875 (1993).

[23] R. H. Swendsen and Jian-Sheng Wang, Phys. Rev. Lett. **58**, 86 (1987).

[24] D. Kandel and E. Domany, Phys. Rev. B **43**, 8539 (1991).

[25] H. G. Evertz, Advances in Physics **52**, 1 (2003).

[26] A. Yanagawa and J. F. Nagle, Chem. Phys. **43**, 329 (1979).

[27] U. Wolff, Phys. Rev. Lett. **60**, 1461 (1988).

[28] We denote numbers of lattice points in $\Lambda_{\rm p}$ and $\Lambda_{\rm d}$ as $|\Lambda_{\rm p}|$ and $|\Lambda_{\rm d}|$, respectively.

[29] M. Kikuchi and N. Ito, J. Phys. Soc. Jpn. **62**, 3052 (1993).

[30] See also H. Müller-Krumbhaar and K. Binder, J. Stat. Phys **8**, 1 (1973); M. P. Allen and D. J. Tildesley, *Computer Simulation of Liquids* (Oxford Science Publications, Oxford, 1987), Chap. 6.

[31] R. W. Youngblood and J. D. Axe, Phys. Rev. B **23**, 232 (1981).

[32] S. Yoshida, K. Nemoto, and K. Wada, J. Phys. Soc. Jpn. **71**, 948 (2002).

[33] C. L. Henley, Phys. Rev. B **71**, 014424 (2005).

[34] P. W. Debye and E. Hückel, Phys. Z. **24**, 185 (1923).

[35] The coulomb potential stemming from the dipolar interactions is $V_{\rm dip} \propto \mu_0 \rho(d)\rho(d')/\|\mathbf{x}(d) - \mathbf{x}(d')\|$.

[36] S. Powell, Phys. Rev. B **87**, 064414 (2013).